Evidence of locally enhanced target heating due to instabilities of counter-streaming fast electron beams

Petra Koester,[1] Nicola Booth,[2] Carlo A. Cecchetti,[1] Hui Chen,[3] Roger G. Evans,[4] Gianluca Gregori,[5] Luca Labate,[1,6] Tadzio Levato,[1,7,a)] Bin Li,[5] Mikako Makita,[8] James Mithen,[5] Christopher D. Murphy,[5] Margaret Notley,[9] Rajeev Pattathil,[9] David Riley,[8] Nigel Woolsey,[2] and Leonida A. Gizzi[1,6]
[1]*Intense Laser Irradiation Laboratory at INO, CNR, Pisa, Italy*
[2]*Physics Department, University of York, York, United Kingdom*
[3]*Lawrence Livermore National Laboratory, Livermore, California 94550, USA*
[4]*Imperial College London, London, United Kingdom*
[5]*Physics Department, University of Oxford, Oxford, United Kingdom*
[6]*INFN, Sezione di Pisa, Pisa, Italy*
[7]*University of Rome Tor Vergata, Rome, Italy*
[8]*Physics Department, Queens University Belfast, Belfast, United Kingdom*
[9]*Rutherford Appleton Laboratory, STFC, Didcot, United Kingdom*

(Received 26 June 2014; accepted 13 January 2015; published online 2 February 2015)

The high-current fast electron beams generated in high-intensity laser-solid interactions require the onset of a balancing return current in order to propagate in the target material. Such a system of counter-streaming electron currents is unstable to a variety of instabilities such as the current-filamentation instability and the two-stream instability. An experimental study aimed at investigating the role of instabilities in a system of symmetrical counter-propagating fast electron beams is presented here for the first time. The fast electron beams are generated by double-sided laser-irradiation of a layered target foil at laser intensities above 10^{19} W/cm^2. High-resolution X-ray spectroscopy of the emission from the central Ti layer shows that locally enhanced energy deposition is indeed achieved in the case of counter-propagating fast electron beams. © *2015 AIP Publishing LLC*. [http://dx.doi.org/10.1063/1.4907195]

The propagation of fast electrons generated in high-intensity laser-matter interactions into the underlying solid target material is accompanied by the emission of X-rays and energetic particles. The typical fast electron currents injected into the target material largely exceed the Alfvèn limit. The transport of such high currents requires the onset of a neutralizing cold electron return current, namely, a counter-streaming electron beam. This scenario applies to a variety of laser-target configurations including proton[1,2] and X-ray sources[3] and the fast ignition scheme to inertial confinement fusion.[4] The understanding of the dynamics of counter-streaming particle beams is important in astrophysical phenomena such as gamma ray bursts, since colliding plasmas are thought to be responsible for magnetic field generation and particle acceleration[5] and are invoked to explain magnetic field generation in the universe.[6,7]

The propagation of fast electrons has been extensively studied to investigate the divergence[8] and the characteristics of the energy deposition[9,10] of the fast electron beam. Recently, the collimation effect due to magnetic fields was also investigated.[11–13]

In a typical laser-solid experiment, the fast electron beam density is some (typically large) fraction of the relativistic critical density to the laser, defined as $n_c = \gamma \frac{m_e}{4\pi e^2} \omega_L^2$, where ω_L indicates the frequency of the laser light, γ is the averaged Lorentz factor of the single electron motion in the laser field, and m_e and e are the mass and the charge of the electron. Thus, the maximum fast electron density ($n_c = 3.3 \times 10^{21}$ cm^{-3} for a laser wavelength of 1 μm and a laser intensity of 2×10^{19} W/cm^2) is much lower than the background electron density in the solid with $n_e > 1 \times 10^{23}$ cm^{-3} and a high-density, low-energy collisional return current is set up in the material to ensure the current neutrality condition, $en_b v_b + en_p v_p = 0$, where the subscript b refers to the beam electrons and p to the background electrons, and e,n and v indicate the electron charge, density, and drift velocity, respectively.

In such a system of counter-streaming electron currents, beam-plasma instabilities, such as the current-filamentation instability and the two-stream instability can grow efficiently transferring kinetic energy from the electron beam into electromagnetic field energy.[14–16] The two-stream instability is a purely electrostatic instability with the wave vector of the growing waves in the direction of the electron beam propagation and thus leading to a longitudinal modulation of the electron density. It dominates the spectrum of unstable modes in the case of diluted non relativistic electron beams. For relativistic fast electron beam velocities, the two-stream instability is overcome by the electrostatic oblique mode instability, with the wave vector of the instability at some angle with respect to the electron beam flow. Both instabilities saturate through electron trapping. The current-filamentation instability dominates the spectrum of unstable modes for counter-streaming electron beams with similar density and moderately relativistic drift speed. The origin of

[a)]Present address: Institute of Physics AS CR, Prague, Czech Republic.

the current-filamentation instability lies in the deflection of the electrons in the transverse magnetic field perturbations, which in turn enhance the magnetic field perturbations. The current-filamentation instability leads to filamentation of the electron beams. Thermalization of the electron flow occurs in this case mainly through merging of the filaments.

Here, we focus on a symmetric system of counter-streaming electron beams to investigate the effect of instabilities. The spectrum of unstable modes for such systems was extensively studied theoretically in the past (see Ref. 17 and references therein). In the relativistic regime, the most unstable mode for the symmetric case $n_b/n_p = 1$ is transverse to the beam propagation axis, whereas in the general asymmetric case $n_b/n_p < 1$, the most unstable mode is a coupled Weibel-two stream mode with the wave vector oblique with respect to the beam propagation axis.[17] The growth rate of the instability scales with the beam to plasma density ratio. In the limit of cold relativistic beams, the fastest growing mode in the symmetric case is transverse and the growth rate is given by $\delta/\omega_p = \beta\sqrt{2/\gamma}$, where ω_p, β, and γ indicate the plasma frequency, the mean beam velocity (in natural units), and the Lorentz factor of the beam electrons.[17] In our experimental conditions, $\delta/\omega_p = 0.77$. Thus, strong filamentation of the fast electron beams is expected to occur for the symmetric system of counter-streaming beams. This scaling is confirmed by experimental observations where filamentation of the fast electron beam was observed in low-density plasmas.[18–20]

The energy deposition characteristics of the fast electron beam can be modified in this scenario, and the role of the filamentation on the energy transfer from the fast electron beam to the plasma is still subject to much uncertainty and discussion. Numerical and theoretical investigations of electron energy deposition in the context of the filamentation instability are mainly performed for an asymmetric beam-plasma system.[21–25] In 2D particle-in-cell simulations with a beam to plasma density ratio of 0.1, significant energy losses (>80%) related to the filamentation instability were found, mainly due to the merging of filaments,[23] whereas simulations with similar parameters including the two-stream instability resulted in much less important energy transfer due to the filamentation instability.[24] In Ref. 25, the beam stopping time is found to be essentially unaffected by the instability, beam deceleration being enhanced in the early stage and reduced in the final stage. In Ref. 22, it is found that beam energy losses increase with increasing beam to plasma density ratio. Experimental data from "*ad hoc*" experiments are needed to test existing models and simulations.

We performed an experiment to study double-sided irradiation of a solid target in a counter-propagating scheme to investigate the role of instabilities in the heating of the target bulk. Compared to the case of a single-sided irradiation, where a cold electron return current is generated from the plasma background electrons, in the double-sided irradiation scheme two counter-propagating fast electron beams are generated leading to a (quasi-) symmetric scenario of identical counter-streaming fast electron populations (Fig. 1). We use X-ray spectroscopy to evaluate the efficiency of target heating.

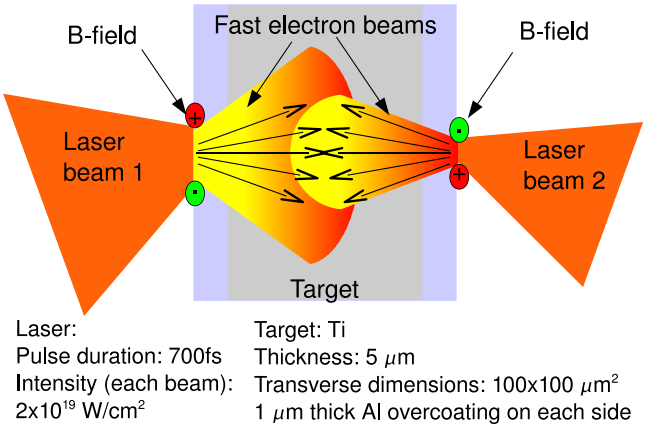

FIG. 1. Schematic of the interaction of two counter-propagating laser beams with a layered solid target.

The experiment was carried out at the VULCAN Petawatt facility. The laser pulse (described in detail in Ref. 26) had an energy up to 400 J with a duration of 700 fs at a wavelength of 1054 nm. In order to obtain two beams for the simultaneous irradiation of either side of the target foil, the main Petawatt beam was split into two beams. One part of the beam was sent to the main focusing off-axis parabola. The second beam was sent to a delay line and focused by another off-axis parabola. The synchronisation between the two beams was performed using an optical streak camera resulting in an uncertainty of 1 ps for the absolute timing between the two beams. In the following, we refer to $\Delta t = 0$ as the nominal zero delay of beam 2 relative to beam 1. This timing is known with ± 1 ps with respect to the actual overlap at target plane. The energy ratio between the two laser beams was measured by means of calorimeters resulting in $E_2/E_1 \sim 1/4$, where E_1 (E_2) is the energy of beam 1 (2). Both beams were focused on the target surface at an angle of incidence of 20° with respect to the target normal forming a triangle. The first beam was defocused in most data shots to ensure overlapping of the beams and to match the intensities. The results reported below refer to an intensity of 2×10^{19} W/cm^2 for both beams.

The targets consisted of 5 μm thick Ti foils coated on both sides with a 1 μm thick Al layer (transverse dimensions 100 μm × 100 μm). The Al coating was used to decouple the plasma X-ray emission from the emission of the propagation Ti layer.

X-ray spectroscopy was performed by means of high-resolution spectrometers based on spherically bent mica crystals. Working in the 5th order of diffraction, the two spectrometers were mounted on either side of the target foil. They were set using the ray-tracing program ORTO[27] to detect a spectral range between 2.3 and 2.8 Å including the Ti emission lines from Lyα to Kα. The simulated positions of the emission lines on the detector plane were fitted with a parabolic function to obtain the dispersion relation. The X-ray spectrometers were equipped with image plate detectors and shielded from noise by means of a lead housing.

The X-ray spectra obtained from the single-sided and double-sided irradiation of the Al coated target foil are displayed in Fig. 2. The spectral range contains the Ti Heα line

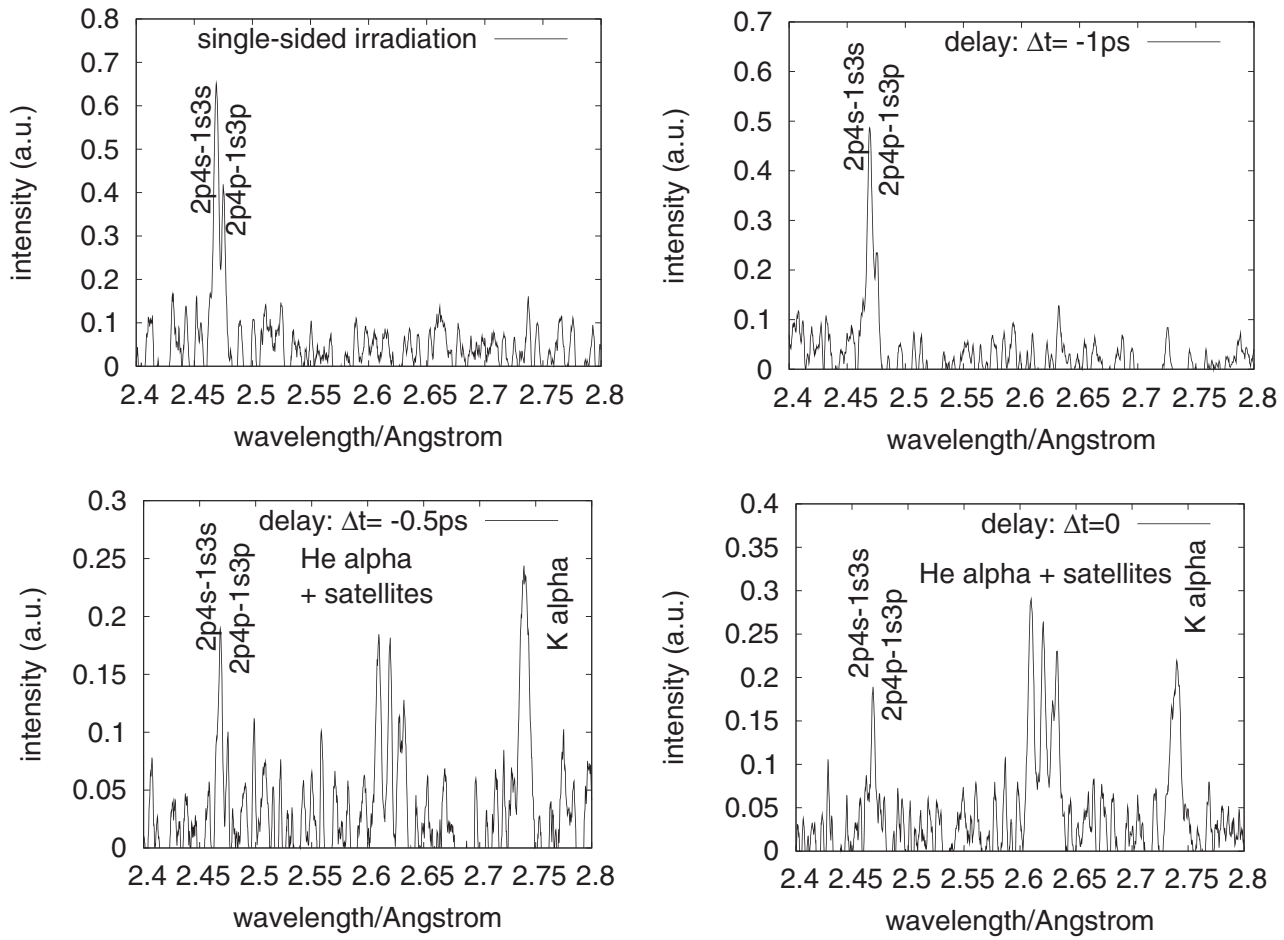

FIG. 2. X-ray spectra obtained from the single-sided and double-sided irradiation of a 5 μm thick Ti foil coated on either side with a 1 μm thick Al layer foil for different time delays between the laser pulses. Transverse dimensions $100 \times 100\ \mu m^2$. (See text for details.)

at 2.610 Å, the intercombination lines at 2.622 Å, and the satellite lines. The Kα line is also visible in the spectrum. The less intense peaks around 2.47 Å are due to double-electron transitions of Li-like ions of the type $2p4s$–$1s3s$ and $2p4p$–$1s3p$.

The delay between the two counter-propagating pulses was varied between different shots by an amount of the order of the laser pulse duration. Here, the experimental results at $\Delta t = -1$ ps (b), $\Delta t = -0.5$ ps (c), and $\Delta t = 0$ (d) are shown. Data shots were repeated for the delays of -1 ps and -0.5 ps confirming the spectral features shown here. The spectrum obtained from single-sided irradiation is also shown (a) for comparison. The X-ray spectra clearly show a dependence on the relative timing of the two counter-propagating beams. The X-ray spectrum at $\Delta t = -1$ ps (b) shows emission only around 2.47 Å from Li-like Ti ions. No Kα emission is visible in the spectrum. These features are very close to those found for single-sided irradiation (a). We point out that a faint Kα line was visible in another spectrum (not shown) obtained with the same delay, indicating that the level of Kα emission intensity for $\Delta t = -1$ ps is close to the noise level.

At $\Delta t = -0.5$ ps, the X-ray spectrum (c) shows a major change, with a contribution from He-like emission lines appearing. Also, the Kα emission is clearly visible in the spectrum. For nominally synchronized beams (d), the intensity of the He-like emission lines increases with respect to the Li-like lines around 2.47 Å. The Kα emission is also present in the spectrum.

A possible explanation for the small Kα signal in the case of single-sided irradiation and double-sided irradiation with a delay of -1 ps with respect to the case of $\Delta t = -0.5$ ps and $\Delta t = 0$ ps might lie in the different fast electron transport properties. In fact, if the fast electrons lose their energy more efficiently in the case of synchronized counter-propagating beams, the cross section for K-shell ionization, having its minimum for moderately relativistic electrons, will increase, thus increasing the number of generated Kα photons.

According to the spectra, the dominant ionization stage of the Ti layer changes for different time delays between the two driving laser pulses indicating a change of the temperature of the Ti layer. The emission from He-like ions and thus the highest target temperature occurs at the delay $\Delta t = 0$ whereas the spectrum at $\Delta t = -1$ ps shows emission only from Li-like ions, indicating a lower target temperature. Since the last-mentioned spectral features are recovered for single-sided irradiation it can be concluded that for the delay $\Delta t = -1$ ps the two generated fast electron beams do not interact significantly.

The cooling of the target is estimated by taking the free streaming limit with flux limiter f: $Q_{fs} = fnvkT$, where n, v, k, and T indicate the electron density, average velocity, Boltzmann constant, and electron temperature. For a flux limiter of 0.06,[28] the energy loss is of the order of 10% in 1 ps. Therefore, heat conduction cannot account for the observed differences.

In principle, refluxing of the fast electron beam(s) inside the target foil may enhance the energy deposition due to recirculating fast electrons spending more time in the target foil. However, refluxing is expected to be suppressed for the case of synchronised double-sided irradiation of the target foil as discussed in Ref. 19. On the other hand, energy deposition due to collisions can play a role only in single-sided irradiation and double-sided irradiation with delayed laser beams due to collisional return currents, while in the case of double-sided irradiation with synchronised laser beams, the fast electron beams constitute a return current to each other and no return current needs to be supplied from the background electrons. These considerations strongly suggest that the observed enhancement of the target temperature in the Ti layer in the case of double-sided irradiation with synchronised laser beams is due to instabilities in the system of counter-propagating fast electron beams.

To estimate the temperature of the Ti layer from the spectra, simulations with FLYCHK[29] were performed assuming an electron density $n_e = 3 \times 10^{23}/cm^3$ and a fast electron fraction of 0.01 at a temperature $T_{hot} = 1$ MeV as expected from the ponderomotive scaling[30] for the experimental laser intensity. Opacity is included in an escape factor approximation. The resulting population of ionization stages shows that He-like Ti is the dominant ionization stage for electron temperatures higher than 600 eV, whereas around 400 eV the Li-like ionization stage is the most populated.

The FLYSPEC code was then used to obtain the expected spectra for different target temperatures to reproduce the spectral features of the X-ray emission at a nominal delay of $\Delta t = 0$. The simulated spectra for three different electron temperatures (600 eV, 700 eV, and 800 eV) are shown in Fig. 3 together with the experimental results at the delay $\Delta t = 0$ in the spectral range between 2.60 and 2.65 Å. The simulated spectra have been normalized to the same intensity for the Heα line. The ratio between the Heα line and the Intercombination line mainly depends on the opacity and is in agreement with the experimental data for a size of the emission region of 5 μm. From a comparison between the simulated spectra at different temperatures in Fig. 3, it can be clearly seen that the intensity ratio of the satellite lines between 2.625 Å and 2.64 Å, and the intercombination line is very sensitive to the target temperature. The best agreement with the experimental data was obtained for a target temperature of 700 eV. The differences between the simulated and the experimental spectrum, particularly pronounced for the intensities of the satellite lines at 2.618 Å and 2.621 Å, might be attributed to unresolved multiplets in the FLYCHK code.

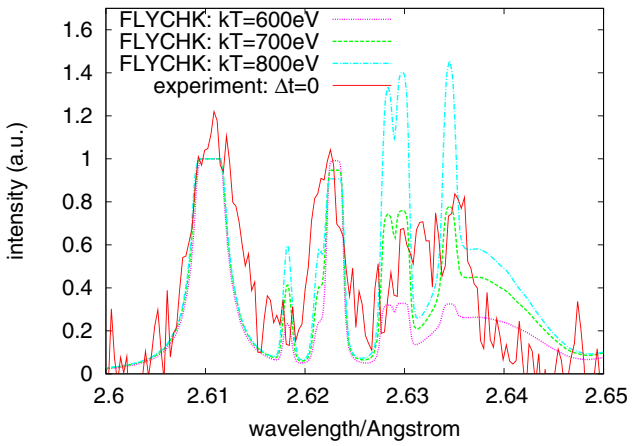

FIG. 3. Emission spectra calculated with FLYSPEC for an electron density of $3 \times 10^{23}/cm^3$ in comparison with the experimentally observed spectrum at the delay $\Delta t = 0$.

Numerical simulations were performed with the LSP code[31] based on a hybrid particle-in-cell/fluid model. In the 2D simulations, fast electrons are injected into a 5 μm thick Ti target foil to model the experimental conditions. The electron distribution had a temperature determined from the ponderomotive scaling and corresponding to a laser irradiation with a pulse duration of 0.5 ps and an intensity of 2×10^{19} W/cm^2. A divergence of 35° half-angle was assumed in the simulations, as measured in similar experiments using the same laser system.[8] The injected fast electron energy corresponds to a conversion efficiency of about 20%. Fig. 4 shows the resulting temperature (top), magnetic field (center), and fast electron density (bottom) maps for single-sided injection for beam 1 (left) and double-sided injection at the peak of the laser pulse. Similar simulations (not shown here) were performed with a single fast electron beam having the same overall energy as the two electron beams in the case of double-sided injection, and the simulation results are consistent with the results presented here.

From the comparison of the two temperature maps, it is clearly visible that localized regions of the target foil reach a higher target temperature in the case of double-sided injection compared to the sum of the two temperature maps resulting from single-sided injection. In fact, a significant change of the fast electron beam dynamics occurs for double-sided injection with respect to single-sided injection. Filamentation of the fast electron beam is much more pronounced in the case of two counter-propagating fast electron beams with respect to a single fast electron beam, as shown by the fast electron density and the magnetic field maps. The counter-propagating fast electron beams are transported in filaments over the whole target thickness and the fast electron flow is confined in a narrow channel. In contrast, the single fast electron beam density does not show a clear filamentary structure. This is also particularly evident in the magnetic field maps. In the case of double-sided injection, the azimuthal magnetic field develops in the region where the two beams overlap reaching its maximum value of about 150 MG at the center of the target foil. In the case of single-sided injection, the magnetic field develops only at the rear side of the Ti layer and is approximately a factor of 4 weaker than in the case of counter-propagating beams.

The energy deposition characteristics are also changed significantly in the two cases. Although the overall deposited

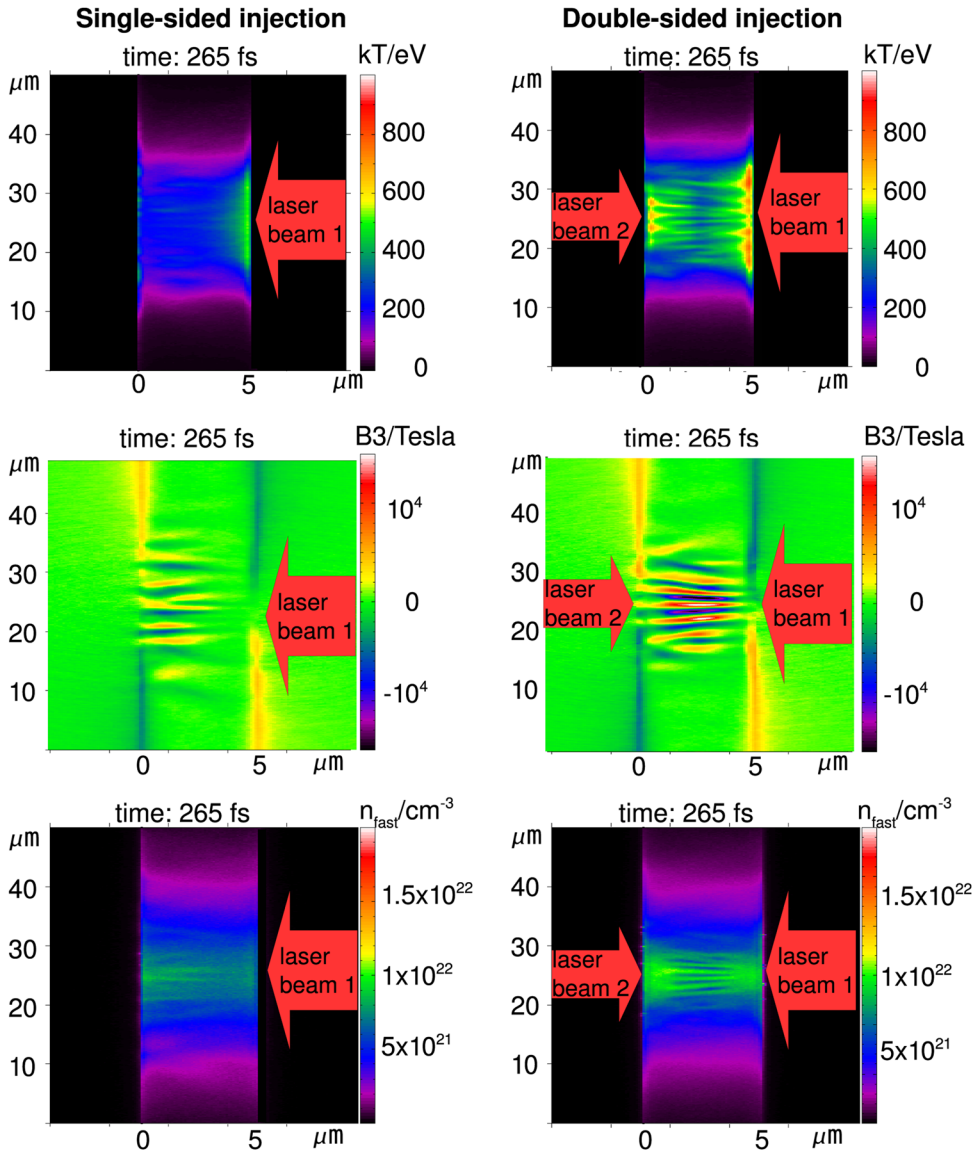

FIG. 4. Temperature (top), magnetic field (center), and fast electron density (bottom) maps just after the peak of the laser pulse (265 fs) as obtained from LSP simulations for a single electron beam corresponding to the irradiation with laser beam 1 (left) and for two counter-propagating electron beams (right) in a 5 μm thick Ti target. (See text for details.)

energy in the target foil is only marginally greater in the case of the two counter-propagating fast electron beams with respect to the single beam, the temperature map resulting from double-sided injection shows a filamentary structure and the temperature is locally strongly enhanced up to 800 eV or more, while in the single-sided injection, the highest temperature does not exceed 550 eV. We also point out that according to Fig. 4, the heat is transported deeper into the target in the case of double-sided injection with respect to the single fast electron beam, where only the surface layer is heated significantly. In fact, according to Fig. 4 (top right), effective heating involves a few μm of the target depth. This value is consistent with the 5 μm emission size estimated from opacity considerations.

In conclusion, evidence of enhancement of local energy deposition due to the interaction of counter-propagating fast electron currents in ultraintense laser interaction was found for the first time. Numerical simulations suggest that the enhanced heating might be attributed to the filamentation current instability leading to significant changes in the fast electron energy deposition and to a locally enhanced target temperature. Our experiment also demonstrates that the counter-propagating scheme presented here is uniquely suited for the study of the fundamental physics involved in a system of counter-streaming beams. Moreover, it is a promising candidate for the efficient generation of hot dense matter, which is of great interest for the study of radiative and transport processes in inertial confinement fusion and astrophysics research.

We would like to thank Ch. Spindloe and coworkers for the preparation of the target foils. We would also like to thank F. Califano for fruitful discussions. The authors acknowledge support from the LASERLAB EUROPE Transnational Access Programme (Grant Agreement No. 228334), the HiPER Project (Grant Agreement No. 211737), and MIUR-PRIN 2012 (Contract No. PRIN2012AY5LEL).

[1]J. Fuchs, P. Antici, E. d'Humieres, E. Lefebvre, M. Borghesi, E. Brambrink, C. Cecchetti, M. Kaluza, V. Malka, M. Manclossi, S. Meyroneinc, P. Mora, J. Schreiber, T. Toncian, H. Pepin, and P. Audebert, Nat. Phys. **2**, 48 (2006).
[2]L. Romagnani, J. Fuchs, M. Borghesi, P. Antici, P. Audebert, F. Ceccherini, T. Cowan, T. Grismayer, S. Kar, A. Macchi, P. Mora, G. Pretzler, A. Schiavi, T. Toncian, and O. Willi, Phys. Rev. Lett. **95**, 195001 (2005).
[3]A. Rousse, P. Audebert, J. P. Geindre, F. Falliès, J. C. Gauthier, A. Mysyrowicz, G. Grillon, and A. Antonetti, Phys. Rev. E **50**, 2200 (1994).
[4]M. Tabak, J. Hammer, M. E. Glinsky, W. L. Kruer, S. C. Wilks, J. Woodworth, E. M. Campbell, M. D. Perry, and R. J. Mason, Phys. Plasmas **1**, 1626 (1994).
[5]R. Fonseca, L. Silva, J. Tonge, W. Mori, and J. Dawson, Phys. Plasmas **10**, 1979 (2003).
[6]G. Gregori, A. Ravasio, C. D. Murphy, K. Schaar, A. Baird, A. R. Bell, A. Benuzzi-Mounaix, R. Bingham, C. Constantin, R. P. Drake, M. Edwards, E. T. Everson, C. D. Gregory, Y. Kuramitsu, W. Lau, J. Mithen, C. Niemann, H.-S. Park, B. A. Remington, B. Reville, A. P. L. Robinson, D. D. Ryutov, Y. Sakawa, S. Yang, N. C. Woolsey, M. Koenig, and F. Miniati, Nature **481**, 480 (2012).
[7]F. Miniati and A. R. Bell, Astrophys. J. **729**, 73 (2011).
[8]J. S. Green, V. M. Ovchinnikov, R. G. Evans, K. U. Akli, H. Azechi, F. N. Beg, C. Bellei, R. R. Freeman, H. Habara, R. Heathcote, M. H. Key, J. A. King, K. L. Lancaster, N. C. Lopes, T. Ma, A. J. MacKinnon, K. Markey, A. McPhee, Z. Najmudin, P. Nilson, R. Onofrei, R. Stephens, K. Takeda, K. A. Tanaka, W. Theobald, T. Tanimoto, J. Waugh, L. V. Woerkom, N. C. Woolsey, M. Zepf, J. R. Davies, and P. A. Norreys, Phys. Rev. Lett. **100**, 015003 (2008).
[9]J. J. Santos, A. Debayle, P. Nicolai, V. Tikhonchuk, M. Manclossi, D. Batani, A. Guemnie-Tafo, J. Faure, V. Malka, and J. J. Honrubia, Eur. Phys. J.: Spec. Top. **175**, 71 (2009).
[10]P. A. Norreys, R. H. H. Scott, K. L. Lancaster, J. S. Green, A. P. L. Robinson, M. Sherlock, R. G. Evans, M. G. Haines, S. Kar, M. Zepf, M. H. Key, J. King, T. Ma, T. Yabuuchi, M. S. Wei, F. N. Beg, P. Nilson, W. Theobald, R. B. Stephens, J. Valente, J. R. Davies, K. Takeda, H. Azechi, M. Nakatsutsumi, T. Tanimoto, R. Kodama, and K. A. Tanaka, Nucl. Fusion **49**, 104023 (2009).
[11]F. Pérez, A. Debayle, J. Honrubia, M. Koenig, D. Batani, S. D. Baton, F. N. Beg, C. Benedetti, E. Brambrink, S. Chawla, F. Dorchies, C. Fourment, M. Galimberti, L. A. Gizzi, L. Gremillet, R. Heathcote, D. P. Higginson, S. Hulin, R. Jafer, P. Koester, L. Labate, K. L. Lancaster, A. J. MacKinnon, A. G. MacPhee, W. Nazarov, P. Nicolai, J. Pasley, R. Ramis, M. Richetta, J. J. Santos, A. Sgattoni, C. Spindloe, B. Vauzour, T. Vinci, and L. Volpe, Phys. Rev. Lett. **107**, 065004 (2011).
[12]F. Zamponi, A. Lübcke, T. Kämpfer, I. Uschmann, E. Förster, A. P. L. Robinson, A. Giulietti, P. Köster, L. Labate, T. Levato, and L. A. Gizzi, Phys. Rev. Lett. **105**, 085001 (2010).
[13]P. A. Norreys, J. S. Green, K. L. Lancaster, A. P. L. Robinson, R. H. H. Scott, F. Perez, H.-P. Schlenvoight, S. Baton, S. Hulin, B. Vauzour, J. J. Santos, D. J. Adams, K. Markey, B. Ramakrishna, M. Zepf, M. N. Quinn, X. H. Yuan, P. McKenna, J. Schreiber, J. R. Davies, D. P. Higginson, F. N. Beg, C. Chen, T. Ma, and P. Patel, Plasma Phys. Controlled Fusion **52**, 124046 (2010).
[14]E. S. Weibel, Phys. Fluids **10**, 741 (1967).
[15]F. Califano, R. Prandi, F. Pegoraro, and S. Bulanov, Phys. Rev. E **58**, 7837 (1998).
[16]F. Califano, D. D. Sarto, and F. Pegoraro, Phys. Rev. Lett. **96**, 105008 (2006).
[17]A. Bret, L. Gremillet, and M. Dieckmann, Phys. Plasmas **17**, 120501 (2010).
[18]M. Tatarakis, F. N. Beg, E. L. Clark, A. E. Dangor, R. D. Edwards, R. G. Evans, T. J. Goldsack, K. D. Ledingham, P. A. Norreys, M. A. Sinclair, M.-S. Wei, M. Zepf, and K. Krushelnick, Phys. Rev. Lett. **90**, 175001 (2003).
[19]M. S. Wei, F. N. Beg, E. L. Clark, A. E. Dangor, R. G. Evans, A. Gopal, K. W. D. Ledingham, P. McKenna, P. A. Norreys, M. Tatarakis, M. Zepf, and K. Krushelnick, Phys. Rev. E **70**, 056412 (2004).
[20]R. Jung, J. Osterholz, K. Löwenbrück, S. Kiselev, G. Pretzler, A. Pukhov, O. Willi, S. Kar, M. Borghesi, W. Nazarov, S. Karsch, R. Clarke, and D. Neely, Phys. Rev. Lett. **94**, 195001 (2005).
[21]G. Shvets, O. Polomarov, V. Khudik, C. Siemon, and I. Kaganovich, Phys. Plasmas **16**, 056303 (2009).
[22]T. Tückmantel, N. Kumar, and A. Pukhov, New J. Phys. **15**, 035021 (2013).
[23]M. Honda, J. M. ter Vehn, and A. Pukhov, Phys. Plasmas **7**, 1302 (2000).
[24]X. Kong, J. Park, C. Ren, Z. Sheng, and J. Tonge, Phys. Plasmas **16**, 032107 (2009).
[25]C. Siemon, V. Khudik, and G. Shvets, Phys. Plasmas **18**, 103109 (2011).
[26]K. L. Lancaster, J. S. Green, D. S. Hey, K. U. Akli, J. R. Davies, R. J. Clarke, R. R. Freeman, H. Habara, M. H. Key, R. Kodama, K. Krushelnick, C. D. Murphy, M. Nakatsutsumi, P. Simpson, R. Stephens, C. Stoeckl, T. Yabuuchi, M. Zepf, and P. A. Norreys, Phys. Rev. Lett. **98**, 125002 (2007).
[27]L. Labate, M. Galimberti, A. Giulietti, D. Giulietti, L. Gizzi, P. Köster, S. Laville, and P. Tomassini, Laser Part. Beams **22**, 253 (2004).
[28]R. Malone, R. McCrory, and R. Morse, Phys. Rev. Lett. **34**, 721 (1975).
[29]H.-K. Chung, M. Chen, W. Morgan, Y. Ralchenko, and R. Lee, High Energy Density Phys. **1**, 3 (2005).
[30]S. C. Wilks, W. L. Kruer, M. Tabak, and A. B. Langdon, Phys. Rev. Lett. **69**, 1383 (1992).
[31]D. R. Welch, D. V. Rose, B. V. Oliver, and R. E. Clark, Nucl. Instrum. Methods Phys. Res., Sect. A **464**, 134 (2001).